Radioluminescence and recombination processes in BaF_2:Ce

2000 J. Phys.: Condens. Matter 12 4097

(http://iopscience.iop.org/0953-8984/12/17/315)

J. Phys.: Condens. Matter **12** (2000) 4097–4124. Printed in the UK PII: S0953-8984(00)09976-8

Radioluminescence and recombination processes in BaF_2:Ce

Andrzej J Wojtowicz†‡§, Piotr Szupryczynski†‡, Jaroslaw Glodo†, Winicjusz Drozdowski† and Dariusz Wisniewski†

† Institute of Physics, N Copernicus University, Grudziadzka 5/7, PL 87-100 Torun, Poland
‡ Chemistry Department, Boston University, 590 Commonwealth Avenue, Boston, MA 02215, USA

E-mail: andywojt@phys.uni.torun.pl

Received 30 November 1999, in final form 4 February 2000

Abstract. In this paper we report measurements of x-ray- and vacuum UV-excited luminescence, luminescence excitation spectra and time profiles, low temperature thermoluminescence and isothermal decays as well as x-ray- and gamma-excited scintillation time profiles and scintillation light yields at various temperatures on BaF_2:Ce and, for reference, on undoped BaF_2, two well known scintillator materials. For the first time we find that all these results can be consistently interpreted in the frame of a model that includes Ce-related recombination centres and several charge 'traps'. The charge trapping at most of these 'traps' has its origin in self-trapping and trapping of holes at regular (V_k) and interstitial (H) fluorine sites. We have identified and characterized two different modes of thermally activated V_k release that precede radiative recombination at Ce sites. These two modes are responsible for a 7 ns rise time and a slower 114 ns components in the scintillation time profile at room temperature (297 K) that produce about 67% of the scintillation light detected within a 0.5 μs time window. The remaining 33% is due to a prompt component decaying with the Ce^{3+} radiative lifetime of about 30 ns that originates from the direct recombination of charge carriers at Ce^{3+} ions. We also estimate that scintillation light loss due to even slower components, at 23.1 μs (H centres), 1.1 ms and 7 ms (V_{kA} and $V_{kA'}$ centres), exceeds at least threefold the amount of light emitted in the 0.5 μs time window. Therefore in addition to their well known role as defect centres actively participating in the formation of stable radiation damage centres these species are also involved in the radiative recombination process itself. The perspectives of improvements in performance of the BaF_2:Ce scintillator are also briefly discussed.

1. Introduction

Radioluminescence is widely used for detection of ionizing radiation in high energy and nuclear physics, astro- and geophysical surveys, nuclear medicine and industry. New Ce-activated scintillator materials have been discovered and are being extensively studied [1]. Positron emission tomography (PET) serves as a good example of high expectations put nowadays on scintillator parameters such as fast scintillation time profiles and high scintillation light yields [2, 3]. New high energy physics experiments at the 1 TeV energy scale require speed (60 MHz interaction rate), extreme radiation hardness and low cost, as projected crystal volumes measure up to 26 m^3 [4].

Although the hyped interest in BaF_2, the fastest known inorganic scintillator material, collapsed soon after the SSC project was abandoned, the material is still being used in specialized electromagnetic calorimeters [5] as well as, occasionally, in some high timing

§ Corresponding author. Address: Institute of Physics, N Copernicus University, Grudziadzka 5/7, PL 87-100 Torun, Poland.

0953-8984/00/174097+28$30.00

resolution PET designs [3] and receives a fair amount of attention from both experimental [6–8] and theoretical perspectives [9]. On the other hand BaF_2:Ce, originally proposed by Czirr and Catalano [10] as a substitute for BaF_2 [11], has never been seriously considered for PET or high energy physics applications. Nevertheless, BaF_2:Ce is a reasonably fast and rugged scintillator material offering a decent stopping power, favourable refraction index and availability of large size crystals [12]. With the sole exception of the less dense and much slower CaF_2:Eu, it is also the most efficient of all the rare-earth-doped alkaline earth fluorides [13]. It does not therefore come as a surprise that BaF_2:Ce has received considerable attention and become a subject of very detailed studies [14–16].

Despite a long history of research aimed at alkaline earth fluorides [17, 18] the mechanism of radioluminescence production in scintillators based on those materials still remains the subject of some controversy. On one hand it was suggested a long time ago [19] that the mechanism of thermoluminescence production in alkaline earth fluorides activated with rare earth ions involves radiative recombination of previously separated (trapped) electrons and holes. On the other hand it is also widely accepted that in pure wide bandgap highly ionic materials the efficient scintillation is almost always due to radiative decay of self-trapped excitons, STEs (see, e.g., [20]). The extremely fast rate of self-trapping and, consequently, the fast rate of STE production has prompted Visser *et al* [15] to propose that almost all of the cerium luminescence of the x-ray-excited BaF_2:Ce is due to the energy transfer from the STE and CVL (core-to-valence luminescence) centres to Ce ions. Nevertheless the significance of excitonic effects for the host-to-ion energy transfer in Ce- and Eu-activated fluoride scintillators has been questioned and it has also been argued that consecutive capture and recombination of charge carriers (not necessarily free band carriers) at rare earth ions provide the mechanism that dominates radioluminescence production in those materials (see e.g. [21]).

In the context of this dispute it is interesting to note that an extremely fast (at about 500 fs) build-up of transient absorption in SrF_2 under two-photon excitation led Thoma *et al* [22] to point to the alternative mechanism of F-centre production in undoped alkaline earth fluorides earlier suggested by Catlow [23]. Catlow considered both the standard exciton collapse mechanism and a novel one, by which conduction band electrons *promptly, spontaneously, and independently of holes* self-trap creating F centres and nearby I centres (interstitial fluorine ions) rendering the electron–hole pairing inessential for the process of radiation defect production in pure alkaline earth fluorides. Since usually a defect production represents only a low efficiency alternative process accompanied by a much more efficient radiative recombination process, it seems very likely that in the rare-earth-doped alkaline earth fluorides an extension of the same mechanism involving rare earth ions provides an efficient channel of radiative recombination generating a 3+ rare earth ion emission that does not require any contribution from excitons.

In the last few papers we have presented a novel approach to the scintillation mechanism in aluminate scintillators that includes measurements of thermoluminescence (TL, at and above 300 K), low temperature thermoluminescence (ltTL, 10 to 350 K), scintillation light yield against temperature (LY–T) and scintillation time profiles (STPs) at various temperatures [24–26]. All these experiments are then consistently interpreted in the frame of a simple model that includes one recombination centre (Ce^{3+}) and a number of electron traps, and evolves under first order kinetics. The more rigorous treatment in which general second order and simplified first order kinetics were considered has also been proposed by Lempicki and Bartram [27]. Both models successfully explain some peculiar features of aluminate scintillators as well as differences and similarities between their Lu- and Y-based varieties [25, 27, 28].

We have applied the same approach to BaF_2:Ce. The initial investigations have been reported in [29]. The conclusion of that work is that slower components responsible for significant differences between scintillation and photoluminescence time profiles of BaF_2:Ce at 297 K (RT) are due to shallow traps. Nevertheless there is also a considerable prompt fast component decaying with the radiative Ce^{3+} lifetime of about 30 ns. While the mechanism by which the fast Ce^{3+} component originates has not been discussed it is obvious that most of it is produced via direct radiative recombination of previously separated charge carriers at Ce^{3+} ions with no contribution from traps.

In this paper we supplement these initial investigations and report results of more detailed and comprehensive studies of BaF_2:Ce. These studies include measurements of radioluminescence spectra, VUV excitation spectra of various BaF_2:Ce emissions, VUV- and UV-excited emission spectra, pulsed VUV-, UV- and x-ray excited time profiles of the Ce emission, scintillation time profiles and scintillation light yields under gamma excitation for various temperatures, low temperature thermoluminescence (ltTL) and isothermal phosphorescence decays (ITDs). All these results are subsequently interpreted using a first order or a simple mixed order kinetic model. The implications for the scintillation mechanism in the rare-earth-doped alkaline earth fluorides are then discussed briefly as are the prospects of improving the performance of the BaF_2:Ce scintillator material.

2. Crystals and experimental details

The crystals of undoped and Ce-doped BaF_2 were grown by Optovac Inc (North Brookfield, MA, USA) using the Bridgman method. Most experiments were performed on crystals from the boule for which the concentration of Ce dopant in the melt was 0.2 mol%. The individual samples were of high optical quality, clear, displayed no colour and no indication of oxygen contamination, and were not subjected to any chemical reducing procedure.

The steady state radioluminescence spectra were recorded at room temperature using a standard set-up consisting of an x-ray tube operated continuously at 35 kV and 25 mA, a monochromator (Acton Research Corporation SpectraPro-500) and a photomultiplier (Hamamatsu R928). The experiment was controlled by a PC. The spectra were not corrected for the spectral sensitivity of the system.

The VUV experiments (luminescence and excitation spectra, pulsed VUV-excited emission time profiles) were conducted at the Superlumi station of HASYLAB, Hamburg, Germany. A detailed description of Superlumi's experimental facilities was given by Zimmerer [30] and is also available on-line [31].

The ltTL glow curves were measured using a closed-cycle double compressor He cooler with a programmable heater. Prior to TL runs the samples were irradiated for about 18 hours by an x-ray source (^{109}Cd) at 4 K. During TL runs the heating rate was kept constant at 9 K min^{-1}. The ITD experiments were performed using a different heating cycle; the sample was irradiated at 4 K and then the temperature was raised to some predetermined higher value and held there for an appropriate time up to 1000 s during which the intensity of emission released from the sample was measured and recorded against time.

The scintillation time profiles were measured at selected temperatures using a set-up based on a standard closed-cycle He cooler with a sample chamber adapted to accommodate a γ-radioactive source (^{137}Cs). A standard synchronous photon counting method was used to record time profiles of γ-excited emission pulses. The temperature of the sample was controlled by a temperature controller in the range of 20–350 K. The same set-up was used to measure scintillation light yields against temperature. A more detailed description of the light yield measurements is given in [25].

Longer decay times (in ms range) of x-ray-excited emission time profiles were measured using a radioluminescence set-up with an x-ray beam modulated by a mechanical chopper and a photon counter (Stanford Research Systems SR 400) working in a boxcar mode. This experiment was performed only at room temperature.

3. Results and discussion

3.1. Radioluminescence

In figure 1 we present radioluminescence spectra of undoped BaF_2 and two Ce-doped (0.03% Ce and 0.2% Ce) BaF_2 crystals measured at room temperature. The spectra show the so-called core-to-valence luminescence (CVL) at about 190 and 220 nm [32], self-trapped exciton (STE) emission [33, 34] and Ce emission consisting of the two ground state component ($J = 7/2$ and $5/2$) peaks at about 310 and 323 nm. The spectra illustrate the effect of Ce^{3+} absorption bands, at 290 and 205 nm, on all emissions in that range including the Ce^{3+} emission itself. The effect is enhanced by the transmission geometry that was used in radioluminescence measurements. We note that with increasing Ce concentration the contribution of Ce^{3+} emission also increases so that the Ce emission gradually replaces the STE emission. The spectrum of BaF_2:0.2% Ce consists almost entirely of the Ce emission although we note that absorption-distorted remnants of the STE emission give evidence that self-trapped excitons are generated by a continuous x-ray excitation and contribute to the radiative deexcitation either directly, via radiative decay, or indirectly, through radiative and/or nonradiative energy transfer processes to Ce^{3+} ions [15].

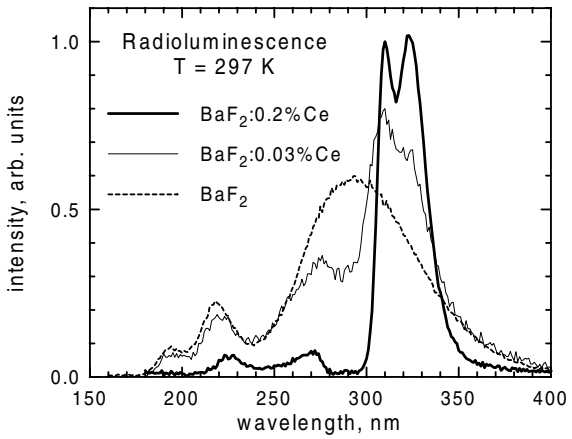

Figure 1. Radioluminescence spectra of BaF_2 (dashed line), BaF_2:0.03% Ce (solid thin line) and BaF_2:0.2% Ce (solid thick line) at room temperature (297 K). The samples were excited by a cw x-ray beam from an x-ray tube operated continuously at 35 kV and 25 mA. The spectra were not corrected for spectral sensitivity of the set-up.

3.2. VUV spectroscopy and time profiles

3.2.1. Luminescence and luminescence excitation spectra. Unlike radioluminescence spectra that simply reflect the dominant radiative relaxation mode by which gamma- or x-ray-generated electronic excitations of the material decay, the photoluminescence spectra may vary strongly depending on the wavelength of the exciting light. In figures 2–4 we show excitation and

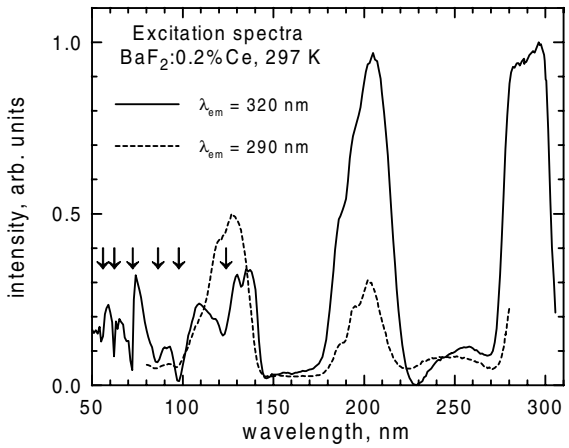

Figure 2. Excitation spectra of STE emission at 290 nm (dashed line) and Ce^{3+} emission at 320 nm (solid line) in BaF_2:0.2% Ce at room temperature. Arrows indicate maxima in the reflectance spectrum of BaF_2. The spectra were corrected using the salicylate standard.

emission spectra obtained for the sample of BaF_2:0.2% Ce under the pulsed synchrotron excitation as described earlier. The excitation spectra (figure 2) were measured at two different emission wavelengths, 290 nm, to which the dominant contribution comes from the STE radiative decay, and 320 nm, reflecting mostly the Ce^{3+} radiative decay. At the longer wavelength range of 170 to 300 nm the spectra show two well known broad bands peaking at about 205 and 290 nm that correspond to f–d transitions of Ce^{3+} ions at nearly cubic symmetry characteristic of the cation site in alkaline earth fluorides [17]. As expected the Ce contribution to emission detected at 290 nm and, consequently, the presence of the f–d bands in the 290 nm excitation spectrum, is much less pronounced than in the second spectrum, taken at 320 nm.

At the shorter wavelength range of 50 to 150 nm, the excitation spectra of the BaF_2:Ce are more likely to reflect various processes by which the host-to-ion energy transfer can occur [35]. Interestingly, the 320 nm excitation spectrum of figure 2 displays a rich structure in that spectral region. Note, however, that positions of sharp large peaks in the normal incidence reflectance spectrum of BaF_2 measured by Rubloff [36] and indicated in figure 2 by arrows, coincide well with the minima in the measured excitation spectra, suggesting that many of the features, such as peaks at 135, 130, 110, 90, 74 and 60 nm in the Ce spectrum, and those at 125, 118 and 90 nm in the STE spectrum, may not correspond to any true processes. Nevertheless, we observe that a minimum at 123 nm that we associate with the excitonic transition (and corresponding reflection maximum) at 123.9 nm [36], is significantly deeper in the Ce spectrum giving it an appearance of a broader double peaked structure positioned between 100 and 150 nm in the vicinity of the bandgap. There is also a shift toward longer wavelengths, observed earlier by Loh [37], who reported the Ce-related shift of the absorption edge in BaF_2. These observations indicate that while at room temperature and under a 120–125 nm excitation the STE emission is excited more effectively than Ce emission, the opposite is true in the case of a longer wavelength excitation at, e.g. 135 nm. However, for shorter wavelength excitations, such as 90, 75, 60 and 50 nm, the Ce emission prevails again.

These observations are corroborated further by the emission spectra shown in figures 3 and 4 and obtained on the same sample of BaF_2:0.2% Ce. The spectra demonstrate clearly that (i) the optical excitation in the vicinity of the excitonic transition at 10 eV (123.9 nm) produces emission with significant contributions of both Ce and STE bands (figure 3, 120 and 115 nm

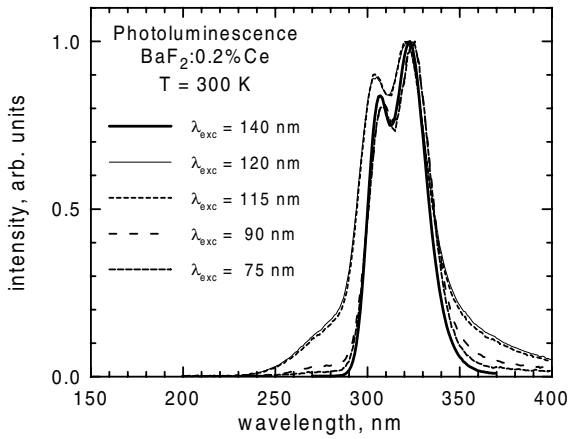

Figure 3. Luminescence spectra of BaF_2:0.2% Ce at room temperature for different excitation wavelengths corresponding to peaks in the excitation spectra shown in figure 2. Note that for excitations in the vicinity of the excitonic transition (at 120 and 115 nm) there is a large STE contribution while shorter and longer wavelength excitations produce emissions dominated by Ce^{3+} bands. The spectra were not corrected for spectral sensitivity of the set-up.

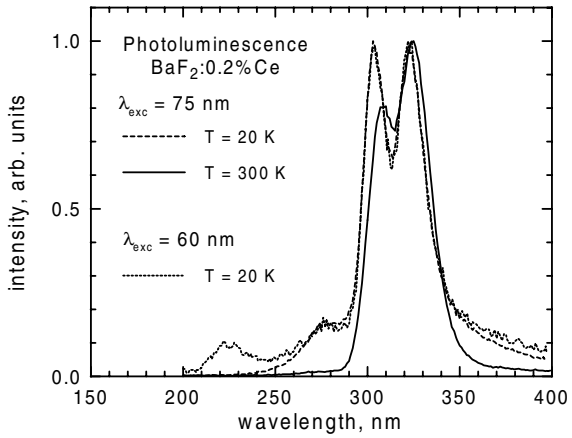

Figure 4. Luminescence spectra of BaF_2:0.2% Ce for the two short wavelength excitations (75 and 60 nm) at two temperatures, 20 and 300 K. Note that the CVL band at 220 nm is visible under 60 nm excitation but is not visible under 75 nm excitation at 20 K. The spectra were not corrected for spectral sensitivity of the set-up.

excitations), (ii) the optical excitation *below* the energy of this transition produces the spectrum with almost *no* STE contribution (figure 3, 140 nm excitation) and, most importantly, (iii) the shorter wavelength excitations of 90 and 75 nm at 300 K produce a spectrum that consists almost exclusively of Ce emission.

Since at 75 nm the exciting photon energy falls short of the threshold energy there is no CVL emission band at 220 nm (compare figures 1, 3 and 4) at any temperature. However, at 20 K and under 60 nm excitation there is a 220 nm CVL band (figure 4). Very likely it is therefore thermal broadening of the adjacent Ce^{3+} absorption band peaking at about 205 nm that is responsible for the absence of CVL emission at ambient temperatures. Note also the distortions of the short wavelength Ce emission band at higher temperatures (figures 3 and 4)

that are similar to those observed earlier in BaF_2 doped with higher concentrations of Ce and due to self-absorption by Ce^{3+} ions [6].

3.2.2. Emission time profiles under pulsed synchrotron excitation. Since there are, in BaF_2:Ce, at least three different luminescence centres (STE, CVL and Ce), each of which has its own radiative decay time, and because of various energy transfer processes that are likely to occur between those centres, it is reasonable to expect that under pulsed synchrotron excitation there will be a corresponding wide variety of emission time profiles.

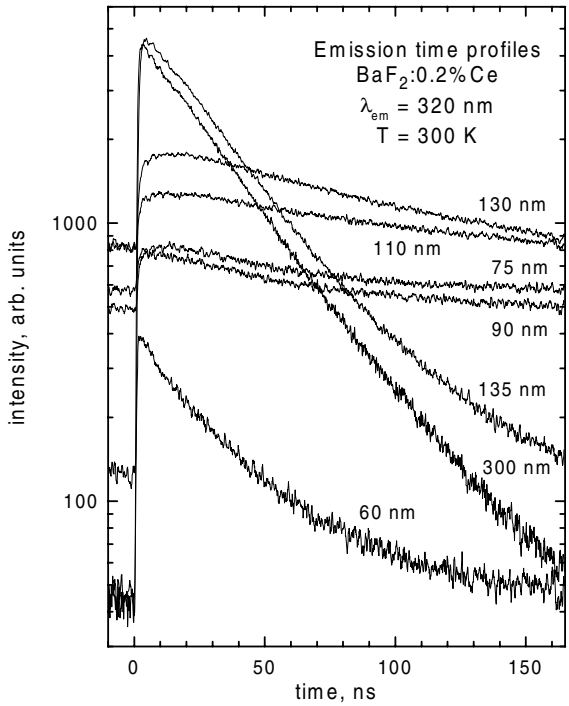

Figure 5. Emission time profiles of BaF_2:0.2% Ce under various wavelength VUV excitations by synchrotron pulses at room temperature. Note the large change between 135 and 130 nm, and then between 75 and 60 nm excitation wavelength time profiles (see text).

In figure 5 we present a selection of emission time profiles of BaF_2:0.2% Ce measured under pulsed synchrotron radiation at the Superlumi station of HASYLAB in Hamburg, using the set-up described earlier. The profiles shown in the figure were measured at one emission wavelength of 320 nm and at one temperature of 300 K, but for a number of excitation wavelengths corresponding to peaks in the excitation spectrum of figure 2. Substantial diversity of rise and decay times in apparently multiexponential time profiles shown in figure 5 indicates that, despite reservations as to the multitude and origin of the peaks in the excitation spectrum, different processes of host-to-ion energy transfer do exist and can be selectively activated by using different excitation wavelengths.

Thus the time profiles excited at one of the f–d absorption bands of Ce^{3+} ions (figure 5, 300 nm excitation, 300 K) show very short rise time and, to a good approximation, single exponential decay of about 33 ns reflecting the direct excitation of Ce ions. At lower temperatures the decay time, at about 27 ns, is shorter and close to the radiative lifetime of the

lowest excited Ce^{3+} d level [15]. Longer decay times measured at higher temperatures (up to 34.2 ns at 350 K), result, most likely, from radiation trapping that has been found responsible for sample thickness and Ce-concentration-dependent variations in measured decay times of BaF_2:Ce [15]. As expected the emission spectrum under the same excitation (not shown) is due exclusively to Ce ions.

For excitation wavelengths that correspond to photon energies below the excitonic transition energy at 10 eV, the rise times become slightly longer but decays are still very nearly single exponential. Decay constants are almost the same as those obtained under the direct excitation of Ce ions, but contributions of slower components are somewhat higher (figure 5, 135 nm excitation). The corresponding emission spectrum is due almost exclusively to Ce^{3+} ions (figure 3, 140 nm). It was suggested earlier the Ce-bound exciton [15, 37] is likely to be responsible for this very efficient and direct channel of energy transfer.

For excitation wavelengths that correspond to photon energies in the vicinity of the excitonic transition at 10 eV, the character of emission time profiles changes drastically (compare 135 and 130 nm profiles in figure 5). A highly unusual convex shape in the entire range of 150 ns, exceptionally long rise times and relatively large contribution of slower components characterizes the time profiles obtained for the 130 and 110 nm excitation (figure 5). The origin of these features, in particular of the long rise time, is not at all clear even though similarly long rise times in the time profiles of STE emission in undoped BaF_2 have been observed earlier [38]. This may be partially due to the fact that the corresponding emission spectra, represented by the 120 and 115 nm excited spectra in figure 3, display both STE and Ce bands and that the origin of Ce emission and its contribution to the time profile is not easy to separate from that of the STE emission. In particular it is quite possible that processes studied in detail by Visser *et al* [15], namely the radiative and non-radiative energy transfers from STE to Ce ions, play a role and contribute to the complexity of measured time profiles.

The next two time profiles shown in figure 5 and measured at even shorter excitation wavelengths of 90 and 75 nm, in addition to dominating slow components reveal some contribution from the fast component that most likely is due to Ce ions. Yet despite the predominance of slow components the corresponding emission spectra show only little contribution from STE (figure 3, 90 and 75 nm). Consequently we conclude that both fast and slow components in the emission time profile excited by 90 and 75 nm are in fact due to emission from Ce ions.

The last profile shown in figure 5 was measured with the shortest excitation wavelength set at 60 nm. This profile, surprisingly, does not follow trends we noted so far. It is clearly much faster showing *more* of the prompt Ce-originated component and *much less* of the slow components that dominated in the preceding time profile measured at 75 nm. Despite this difference the emission spectra obtained at 75 and 60 nm excitations are nearly the same, consisting mostly of the Ce emission and almost none of the STE. The difference between the two profiles is in a relative drop in efficiency of slow processes feeding the Ce ions upon a small decrease of the excitation wavelength.

3.2.3. VUV spectroscopy and time profiles: discussion. The VUV excitation spectra and time profiles of Ce and STE emissions were analysed earlier by Wojtowicz *et al* [39]. They point to a peculiar difference between time profiles obtained at 60 and 75 nm and offer a possible explanation. They note that the photon energy corresponding to the 60 nm wavelength is above, while that for the 75 nm is below the threshold for the Ba^{2+} 5p core excitation and, therefore, below the threshold for excitation of the CVL emission [35]. Consequently the 75 nm excitation creates a valence band hole and a *hot* conduction band electron that have an

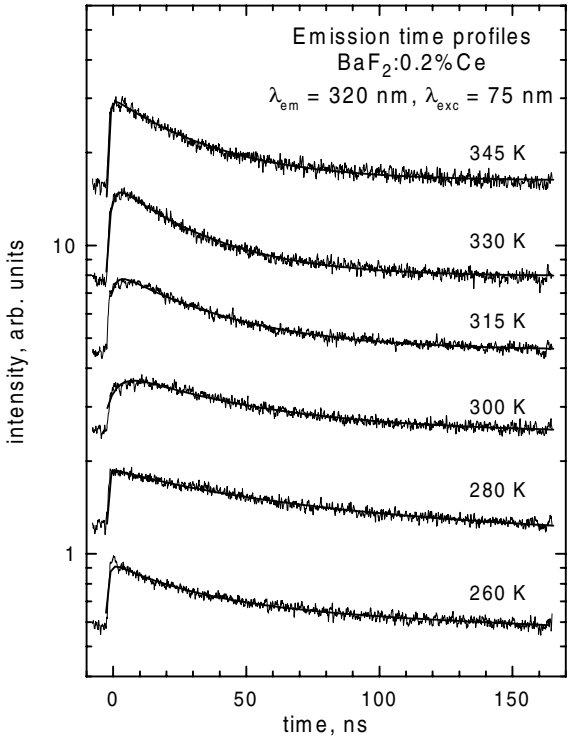

Figure 6. Emission time profiles of BaF_2:0.2% Ce under 75 nm excitation by synchrotron pulses for various temperatures. The consecutive curves have been shifted vertically. The jagged thin solid lines represent experimental traces while the thick solid lines depict two-exponential fits with an additional fitting constant to correct for background and longer decay time components.

opportunity to separate and become trapped. The 60 nm excitation, in contrast, creates a Ba^{2+} 5p core hole and a *cold* electron in the conduction band that are not likely to separate. After a core hole and a valence electron recombine producing a CVL photon and leaving behind a hole in the valence band and an electron in the conduction band, relaxation could conceivably proceed by four different mechanisms: (i) a hole self-traps and an electron is captured leading to STE emission and/or Ce emission after transfer (130 nm type time profile); (ii) a free band electron and hole recombine creating an exciton which subsequently self-traps, generating STE emission and/or Ce emission, again with a 130 nm type profile; (iii) a hole self-traps while an electron is captured by a nearby Ce ion; the net coulombic attraction would then draw the self-trapped hole, which recombines with the Ce^{2+} ion. This could not, however, take place at temperatures below 108 K, where V_k centres are immobile, so that no low-temperature Ce emission would occur; (iv) a hole could be captured by a nearby Ce^{3+} ion, followed by attraction of a free electron and recombination with the Ce^{4+} ion. This would give rise to fast Ce emission at any temperature. Thus only the last option is consistent with all the experimental observations.

The surprisingly different and much faster 60 nm profile is due, therefore, to fast consecutive hole and electron capture and radiative recombination at Ce ions which supports a contention that such a process is possible and that it may play a role under ionizing excitation. On the other hand the slow components in the 75 nm excited time profile are very likely, therefore, due to the charge trapping interfering with the process of recombination of separated

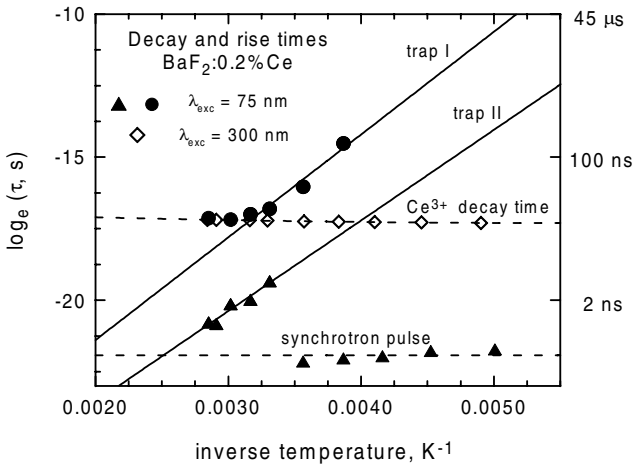

Figure 7. Decay and rise times against the inverse temperature. Points in the diagram were obtained from fits to time profiles shown in figure 6 and represent decay and rise times under 75 nm excitation (filled circles and triangles) and decay times under 300 nm excitation into one of the Ce^{3+} f–d absorption bands (empty diamonds). The solid lines depict straight line fits obtained for selected points while dashed lines indicate rise and decay times determined mostly by synchrotron pulse and Ce^{3+} radiative lifetime, respectively.

charge carriers. Clearly the final effect of the energy transfer process activated at these shorter wavelength excitations resembles the outcome of the gamma- or x-ray-initiated scintillation pulse in BaF_2:Ce that is characterized by a considerable contribution of slower components [29].

This observation makes profiles obtained at 75 nm for a number of temperatures, presented in figure 6, particularly interesting from the point of view of the scintillation mechanism in BaF_2:Ce. In figure 7 we show decay and rise times obtained from fits to those profiles as a function of inverse temperature, $1/T$. For comparison we included also decay times of profiles excited at 300 nm.

From the simple one-trap model we know that a trap can modify a rising or a decaying part of the scintillation time profile [25] introducing a characteristic time τ (trap lifetime):

$$\frac{1}{\tau} = s \exp\left(-\frac{E}{k_B T}\right) \tag{1}$$

where s and E are the frequency factor and trap depth, respectively. This formula can be used to extract trap parameters from the appropriate straight line fits as shown in figure 7. Since there are clearly two different straight lines that fit experimental points we conclude that there are two different traps, designated I and II, that are responsible for longer decays (trap I) and longer rise times (trap II) at relevant temperatures. Although in principle it is possible to find parameters of those traps we will later demonstrate that by including results of other experiments and making one fit to all of the points allows us to improve the quality of each of those two fits considerably.

3.3. Low temperature thermoluminescence (ltTL) and isothermal decays (ITDs)

3.3.1. Low temperature thermoluminescence. In figure 8 experimental points show the ltTL glow curves of undoped and Ce-doped BaF_2 crystals measured at a heating rate of 9 K min^{-1}.

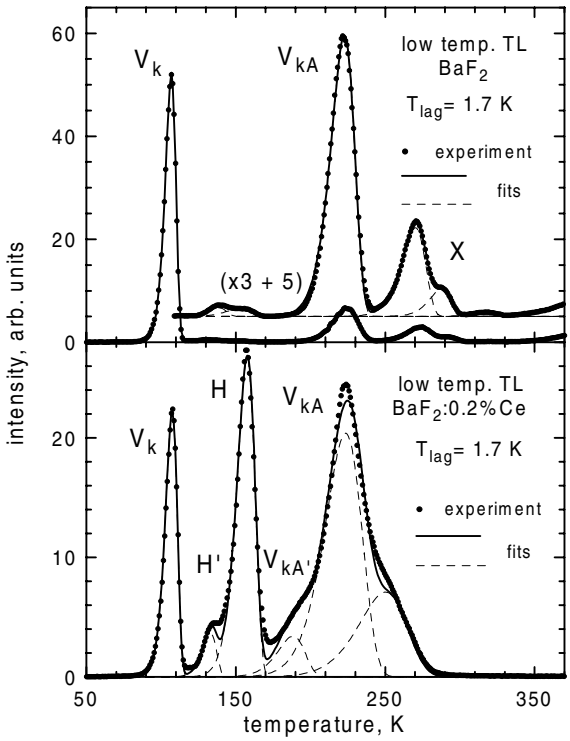

Figure 8. Thermoluminescence glow curves of BaF_2 and BaF_2:0.2% Ce following 18 hour x-ray irradiation at 4 K. The second BaF_2 curve, shifted vertically by five units and multiplied by a factor of three, was measured after 6 hour irradiation at 108 K. Heating rate was 9 K min^{-1} and thermal lag was assumed of 1.7 K for all the glow curves shown in the figure. Filled circles represent experimental points; solid and dashed lines represent TAMTAM fits. Trap parameters obtained from these fits are summarized in tables 1 and 2. The assignment of glow peaks follows earlier work (see text).

Prior to TL runs the samples had been irradiated for 18 hours at 4 K as described earlier, except for the second curve for the undoped BaF_2 crystal that was measured after a 6 hour irradiation at 108 K.

In substantial agreement with previous reports [29, 33, 35, 40–42] we note that the undoped crystal reveals one dominant well known peak at 107 K (V_k centre) and additional weaker features at 223 K (V_{kA} centre) and at 275–290 K (designated X). The Ce-doped crystal glow curve is more complex as the V_k band no longer dominates the spectrum and there are two additional major peaks, at 157 K (H centre, hardly visible in the undoped crystal), and the V_{kA} band at 224 K, and some smaller ones, at 130 K (designated H′), 190 K ($V_{kA'}$) and 250 K. The V_{kA} band in BaF_2:Ce is somewhat broader and it is accompanied by two additional not well resolved but identifiable satellite peaks mentioned above that do not show up in the undoped crystal. We also observe that the V_k band in the Ce-doped crystal is slightly broader and peaks at a higher temperature of 107.8 K. The total TL yield of the Ce-doped crystal (mass 0.17 g) is about 2.5 times higher than that of the undoped crystal (0.30 g). This is consistent with the observation that the undoped alkaline earth fluoride crystals are less readily colourable under ionizing irradiation than their rare-earth-doped counterparts (see e.g. [23, 43, 44]).

Table 1. Trap parameters obtained from the glow curve fitting by the TAMTAM procedure for BaF_2.

Peak number i	Glow peak T_0 (K)	n_{0i}/n_{01}	E_i (eV)	$\ln s_i$
1	106	1.0	0.273	26.45
2	130	0.015	0.183	12.32
3	147	0.018	0.134	6.01
4	224	0.29	0.523	23.03
5	272	0.12	0.762	28.39
6	291	0.04	1.025	36.94
7	316	0.008	0.875	27.85
8	386	0.17	0.864	21.36

Table 2. Trap parameters obtained from the glow curve fitting by the TAMTAM procedure for BaF_2:Ce.

Peak number i	Glow peak T_0 (K)	n_{0i}/n_{01}	E_i (eV)	$\ln s_i$
1	107	1.0	0.245	23.14
2	133	0.19	0.322	24.64
3	157	1.8	0.350	22.05
4	188	0.35	0.321	15.61
5	224	2.84	0.332	12.74
6	250	1.27	0.318	10.01

The procedure by which the exact positions of the peaks (the true peak temperatures) given above were determined will be explained later. We found that the thermal lag, which is the difference between the true sample temperature and that of the heating element, was 1.7 K.

TL fits shown by solid and dashed lines in figure 8 have been obtained by the TAMTAM procedure developed by T M Piters. Since under first order kinetics a complex glow curve can be represented by a sum of single peak terms, each of which is given by the Randall–Wilkins formula [45] this procedure uses the expression:

$$I(T) = \sum_{i=1}^{N} n_{0i} s_i \exp\left(-\frac{E_i}{k_B T}\right) \exp\left(-\frac{s_i}{\beta} \int_{t_0}^{T} \exp\left(-\frac{E_i}{k_B T}\right) \mathrm{d}T\right) \qquad (2)$$

where T is the true sample temperature (corrected for the thermal lag of 1.7 K), β stands for the heating rate, n_{0i}, E_i and s_i are initial occupied trap concentrations, energy depths and frequency factors respectively. The parameters retrieved by this procedure are summarized in table 1 (BaF_2) and table 2 (BaF_2:Ce). Note that despite clear correlations between *positions* of peaks in two materials *trap parameters* assigned to them by the TAMTAM procedure differ substantially. Interestingly this is true not only of those peaks (at 130, 150, 190, 250 K) that are small (or absent) and therefore may prove difficult (or impossible) to fit reliably in one or the other material but also of larger peaks that are clearly visible in both materials (at 108 and 224 K).

Singularly interesting and significant is the difference between frequency factors and energy depths assigned by TAMTAM to the V_k peaks in the doped and undoped crystals. The difference in frequency factors reflects the observed difference in shapes (widths) of those two peaks. As their locations are more or less the same the procedure attempts to compensate for the lower frequency factor in the Ce-doped crystal by an adequate decrease of the energy depth. Surprisingly we find therefore that the V_k peak, well established as the one that corresponds to the *intrinsic* process of thermally induced release of the self-trapped holes in the lattice of the fluoride crystals, displays some unexpected changes upon relatively moderate Ce doping (0.2%). We will discuss this problem later on.

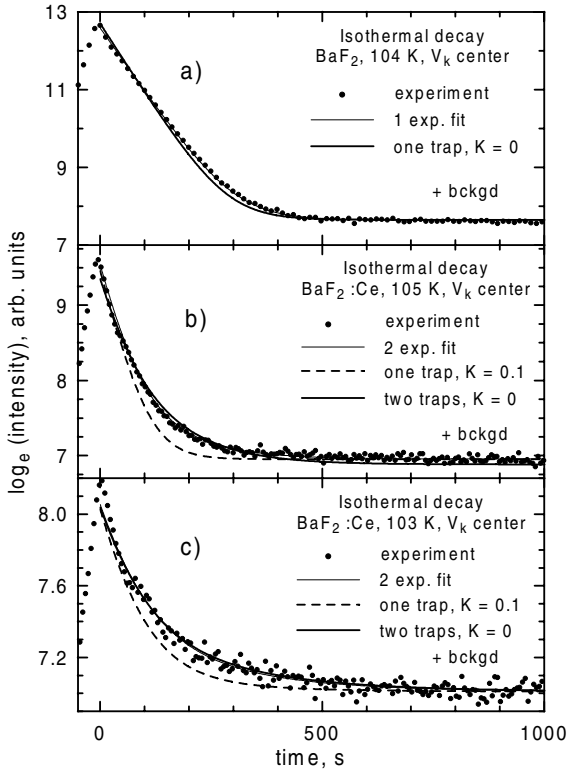

Figure 9. Representative isothermal phosphorescence decay curves of (a) BaF_2 at 104 K, (b) BaF_2:0.2% Ce at 105 K and (c) BaF_2:0.2% Ce at 103 K measured in the vicinity of the V_k glow peak. Full circles represent experimental points, thin solid lines depict one- and two-exponential fits with additional fitting constant to correct for background. Dashed and solid thick lines represent calculated curves with parameters derived by a procedure described in the text (model I and II, see text).

3.3.2. Isothermal decays (ITDs). An alternative experiment that is also capable of providing information on trap parameters is the measurement of phosphorescence isothermal decays. In such an experiment, as described earlier, the sample is irradiated at lower temperature then heated up to some predetermined temperature and held there while the decay of emission released from it is measured against time for up to 1000 s.

In figure 9 we show by experimental points three representative isothermal phosphorescence decays measured in the vicinity of the V_k peak of BaF_2 at 104 K (figure 9(a)), and of BaF_2:Ce at 105 K (figure 9(b)) and at 103 K (figure 9(c)). Note that the undoped crystal decay (figure 9(a)) is well described by a single exponential expression with a variable background (a thin solid line) over more than two orders of magnitude. Quite to the contrary, the decays of the Ce-doped crystals (figure 9(b) and (c)) do not display a prominent one-exponential component and are clearly more complex. A reasonably good fit to these decays can be obtained using a two-exponential expression with a background, shown by thin solid lines.

The isothermal decay measured in the vicinity of the H peak of BaF_2:Ce at 155 K is shown by experimental points in figure 10. Note that the decay has been measured over more than two orders of magnitude and that it is not single exponential. We also observe that a two-exponential fit, shown by a thin solid line, matches reasonably well all the experimental points.

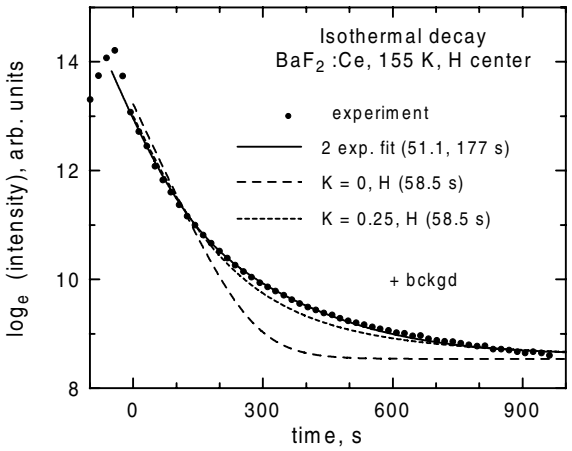

Figure 10. Isothermal phosphorescence decay of BaF_2:0.2% Ce at 155 K measured in the vicinity of the H glow peak. Full circles represent experimental points; the thick solid line depicts two-exponential fits with additional fitting constant to correct for background. Dashed thin lines represent calculated model curves with parameters derived by a procedure described in the text.

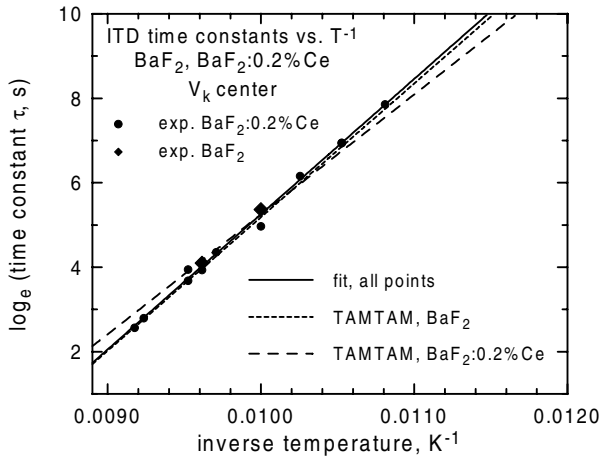

Figure 11. Isothermal decay time constants against the inverse temperature. Points in the diagram were obtained from one-exponential (full diamonds) and two-exponential (full circles) fits to ITD curves of BaF_2 and BaF_2:0.2% Ce, respectively, for various temperatures in the vicinity of the V_k glow peak, such as those shown in figure 9. The solid line represents a straight line fit for all points giving the best estimate of trap parameters (see text). The short and long dashed lines depict calculated straight lines with trap parameters derived from TAMTAM fits to V_k glow peaks of BaF_2 and BaF_2:0.2% Ce, respectively.

The isothermal decays measured at the V_{kA} peak of BaF_2:Ce are, quite predictably, very complex and they will be presented and discussed in a separate paper. The various simulations of V_k and H isothermal decays shown in figures 9 and 10 as well as the significance of the parameter K will be discussed in more detail later on.

In figures 11 and 12 we present summary of measurements of emission decay times obtained for both the BaF_2 and BaF_2:Ce crystals over a large thermal range (25–350 K)

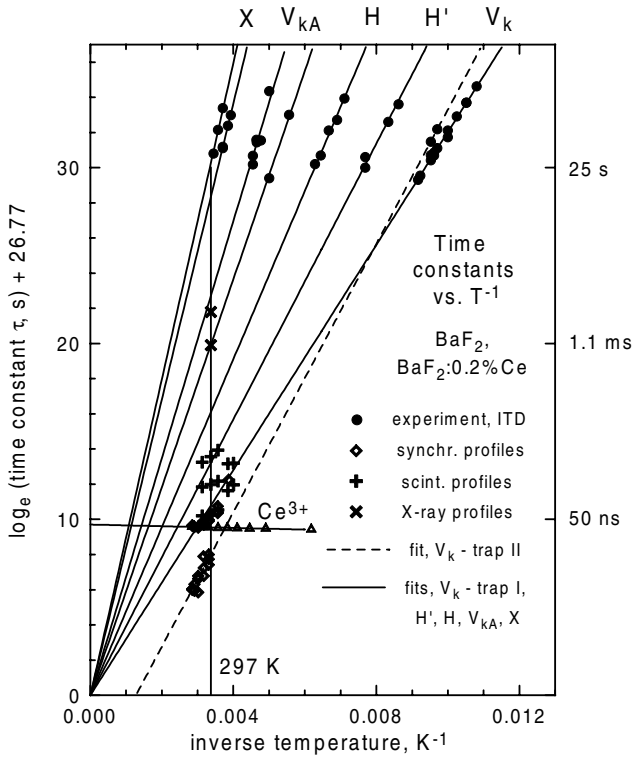

Figure 12. Time constants as a function of inverse temperature. Points in the diagram were obtained from fits to ITD curves (filled circles) measured in the vicinity of all major glow peaks of BaF_2 and BaF_2:0.2% Ce, from fits to emission time profiles under synchrotron excitation of 75 nm (open diamonds), and from fits to scintillation time profiles under γ and x-ray excitations (+, $\times$ respectively). Solid lines depict straight line fits to points corresponding to different glow peaks under assumption of a common frequency factor (see text). The dashed line represents a straight line fit to points corresponding to second exponential components of ITD BaF_2:0.2% Ce decays shown in figure 9(b) and (c) and rise times in synchrotron excited time profiles. A horizontal solid line represents a straight line fit to points (open triangles) obtained from fits to Ce^{3+} emission profiles under the 300 nm excitation (into the f–d absorption band). Note that points in this diagram obtained from fits to various experimental time profiles, span 11 orders of magnitude in time (from a 1 ns rise time to about 100 s ITD decay time). A vertical solid line represents a temperature of 297 K.

in various experiments. In these figures the natural log of decay times derived from the appropriate fits is plotted against the inverse temperature and, since the trap lifetime is given by formula (1), all the points that are related to the same trap should fall on the same straight line.

In figure 11 we plot decay times derived from one- or two-exponential fits to measured ITD curves of BaF_2 (diamonds) and BaF_2:Ce (filled circles). Only the dominant shorter decay time was included as a point in the figure in the case of two-exponential decays. In principle, as explained above, the straight line fits to points obtained for BaF_2 and BaF_2:Ce should yield trap parameters s and E that are characteristic of the traps in these two materials. Remarkably the fits yield parameters that are within reasonable limits identical to themselves as well as to the parameters obtained from the fit to all the points, for the undoped and Ce-doped samples.

This suggests that there is a unique trap in both materials. The fit to all the points in the figure is shown by a solid line that yields $E = 0.276$ eV and $\ln s = 26.77$ ($= 4.21 \times 10^{11}$ s^{-1}). The other straight lines shown in figure 11 by short and long dashes have been drawn, for comparison, using s and E parameters obtained from the TAMTAM fits to the TL glow curves of BaF_2 and BaF_2:Ce, respectively. Note that the line of BaF_2 falls very close to the solid line and to all the ITD points despite the fact that most of those points have been actually obtained from fits to ITD curves of the Ce-doped, not undoped, sample. Quite to the contrary, the BaF_2:Ce line strays away from the points and all the remaining lines shown in figure 11. We conclude that despite the difference in appearance of ITD curves the thermal dependences of their dominant decay rates do not support the idea of two different traps in the undoped and Ce-doped BaF_2 crystals. The small but persistent difference between the TL glow curves of BaF_2 and BaF_2:Ce in the vicinity of the V_k peak responsible for significant differences of trap parameters derived from the TAMTAM procedure applied to those curves, does not translate into different straight line fits in figure 11. The idea of two different traps in BaF_2 and BaF_2:Ce is not consistent with ITD fits. The difference between TL glow curves of the two materials remains unexplained.

The time constants plotted in figure 12 were obtained from various experiments, including ITD measurements at temperatures in the vicinity of all the major BaF_2 and BaF_2:Ce TL glow peaks. The ITD points are shown by filled circles, rise and decay times of Ce-emission under pulsed synchrotron excitation that have also been included in figure 7 are shown by open diamonds and there are also decay times of Ce emission measured under gamma and x-ray excitations which are shown by + and $\times$ symbols. Note that the ITD points obtained in the vicinity of the V_k peak include both time constants derived from the two-exponential fits to the ITD curves of BaF_2:Ce taken at 103 and 105 K and shown in figure 9(b) and (c). The straight line fit shown by a solid line and designated V_k is the same as the one shown in figure 11. Although this fit does not include points representing the decay times obtained from time profiles under 75 nm synchrotron excitation they do fall reasonably close to the fit line. This suggests that the same trap is responsible for both the glow peak (and ITD decays) at 107 K and the longer than radiative decay times measured at and above 297 K. We will designate this trap as V_k-I.

The dashed line in figure 12, also designated as V_k, represents a different straight line fit to points obtained from fits to the rise times obtained from the emission time profiles under synchrotron excitation and the decay times of the slower second components obtained from the two-exponential fits to the ITD curves of BaF_2:Ce at 103 and 105 K. Note that the rise time points shown in this figure represent three different sets of fits not just one as in figure 7. Interestingly the straight line fit parameters from figure 7 (trap II) and those obtained from the dashed line of figure 11 are reasonably close. We will designate the hypothetical trap assigned to the dashed line as V_k-II. This trap is, presumably, responsible for the rise times and two-exponential ITD decays measured in the vicinity of the V_k peak in the BaF_2:Ce.

The additional solid lines, designation of which follows those of the peaks in the TL glow curve, H′, H, V_{kA}, and X, represent fits to ITD points obtained at the vicinity of the relevant glow peaks of BaF_2 (X and V_{kA}) and BaF_2:Ce (V_{kA}, H and H′). The straight line fits through the origin were performed after the y-coordinate of all the points had been shifted by a factor of 26.77 which is the frequency factor of the V_k-I trap found from the fit shown in figure 11. As demonstrated in [29] such a procedure is justified under the assumption that all of the included traps share the same frequency factor. The slopes of the lines are then uniquely determined by energy depths of the corresponding traps. In table 3 we summarize trap parameters obtained from all the straight line fits shown in figure 12.

Table 3. Summary of parameters describing traps in BaF_2 and BaF_2:Ce and obtained from fits shown in figure 12. The fit for the V_k-II trap involves both the ITD and rise time points and provides both the frequency factor s and energy depth E. For the remaining traps we assumed the same frequency factor, $s = 4.207 \times 10^{11}$ s^{-1}, obtained from the fit to ITD points of the V_k-I trap shown in figure 11. The energy depths were then obtained from the straight line fits through the origin that included only ITD points shown in figure 12. The glow peak positions T_0 have been calculated using trap parameters obtained from the ITD fits for the 9 K min^{-1} heating rate and under first order kinetics. The trap lifetimes have been calculated at 297 K.

Trap	Glow peak T_0 (K)	E (eV)	ln s	τ (ns)
V_k-I	107	0.276	26.77	114
V_k-II	110	0.329	31.63	7.0
H′	130	0.338	26.77	1.29×10^3
H	158	0.412	26.77	23.2×10^3
V'_{kA}	194	0.510	26.77	1.06×10^6
V_{kA}	220	0.582	26.77	17.3×10^6
X_1 (BaF_2)	273	0.726	26.77	4.79×10^9
X_2 (BaF_2)	291	0.776	26.77	32.9×10^9

3.3.3. Low temperature thermoluminescence and isothermal decays: discussion. The survey of experimental results presented so far reveals some inconsistency in conclusions based on the ltTL and ITD experiments at the V_k TL peaks in BaF_2 and BaF_2:Ce at about 107 K. It is widely accepted that those peaks result from the radiative recombination that is driven by an intrinsic process of thermally activated release of the self-trapped holes or the V_k centres. In this context the occurrence of even small but persistent differences between the TL glow curves in BaF_2 and BaF_2:Ce is particularly annoying and rather difficult to rationalize. Both curves can be reasonably well reproduced using the TAMTAM procedure under the assumption of a single trap and first order kinetics. As noted before, the relatively small difference between the two glow curves translates into quite disparate estimates of parameters s and E that characterize the hole release process in the two materials (two different traps). Although the thermal dependences of dominant decay rates extracted from those curves do not support the notion of the two different traps as shown in figure 11 and discussed before, on the other hand, the marked differences between the ITD curves obtained for the BaF_2 and BaF_2:Ce crystals seem to suggest that kinetics of the recombination process may be different in the two materials.

To reconcile these apparent contradictions we will consider two different hypotheses. Under the first one we assume that there is, as suggested by the ITD fits shown in figure 11, a unique trap in both undoped and Ce-doped fluoride or, in other words, that there is a unique pair of s and E parameters characteristic of both materials. The difference in glow curve shapes and ITD curves would then be due not to different traps but to different recombination kinetics in the two materials, supposedly of first order in BaF_2 and mixed (or second) order in BaF_2:Ce. We will designate this option as model I. Under the second hypothesis (model II) we assume that in addition to the 'ordinary' trap that occurs both in the undoped and Ce-doped materials and is solely responsible for TL and ITD in BaF_2 (V_k-I) there is an additional different trap in BaF_2:Ce that causes broadening of the TL glow curve and contributes the second exponential term to ITD curves of BaF_2:Ce. This second trap would have to be the trap that we have assigned to the dashed straight line fit in figure 12 and designated V_k-II.

We begin by comparing the experimental ltTL glow curves of BaF_2 and BaF_2:Ce with the curves calculated under the two hypothesis discussed above. The procedure we will describe below for BaF_2 will also explain how the thermal lag has been established.

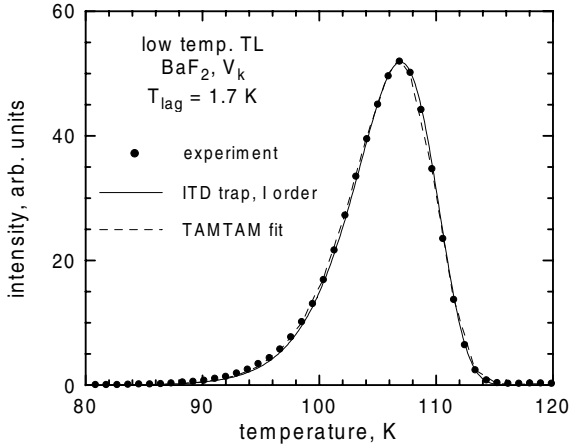

Figure 13. Thermoluminescence glow curve of BaF_2 in the vicinity of the V_k peak following x-ray irradiation at 4 K. Heating rate was 9 K min^{-1}. Filled circles represent experimental points; a dashed line represents the TAMTAM fit and a solid line was calculated with parameters derived from ITD points (figures 11 and 12, table 3) for the trap V_k-I. With the exception of thermal lag (1.7 K) there is no other adjustable parameter.

In figure 13 we show by experimental points the ltTL glow curve of BaF_2 in the vicinity of the V_k peak. A thin solid line has been calculated with no adjusted parameters by numerically integrating the first of the two equations (obtained from simple kinetic equations with binomial terms taken into account and by taking the temperature T as an independent variable [25, 46]):

$$\frac{\partial n}{\partial T} = -\frac{1}{\beta}\frac{n^2}{n+K}s\,\exp\left(-\frac{E}{k_BT}\right) \qquad I(T) = \frac{n^2}{n+K}s\,\exp\left(-\frac{E}{k_BT}\right) \quad (3)$$

and then substituting the solution of the first equation into the second one. In these equations β is the heating rate (0.15 K s^{-1}), k_B is the Boltzmann constant, s and E are the frequency factor (in s^{-1}) and the energy depth (in eV) from the ITD fit (V_k-I, figures 11, 12 and table 3), $n(T)$ and $I(T)$ are the temperature dependent concentration of filled traps (V_k centres) and thermoluminescence intensity, respectively. The order parameter $K = NR/n_0$, where N is the concentration of traps, R stands for the ratio of coefficients describing trapping and recombination rates and n_0 is the initial filled trap concentration [46]. We make a choice of units such that n_0 is equal to 1. Note that for $K = 0$ the equations (3) assume the well known simple form [25, 46]:

$$\frac{\partial n}{\partial T} = -\frac{n}{\beta}s\,\exp\left(-\frac{E}{k_BT}\right) \qquad I(T) = ns\,\exp\left(-\frac{E}{k_BT}\right) \quad (4)$$

that can be solved in a closed form yielding the well known Randall and Wilkins expression for a single trap (see formula (2) representing such an expression for a number of traps).

On the other hand for $K \gg 1$ we obtain:

$$I(T) = n^2 s'\,\exp\left(-\frac{E}{k_BT}\right) \quad (5)$$

which is in fact the second order expression describing thermoluminescence intensity with a modified frequency factor, $s' = s/K$ [46].

The simulated curve calculated as described above (trap parameters from the ITD fit, table 3, trap V_k-I, $K = 0$) matches the experimental points very well after these points have

been shifted by 1.7 K. This takes care of the thermal lag that causes the true sample temperature to be lower than the measured one. In the next step we performed a fit using the TAMTAM procedure that yielded trap parameters (table 1, peak 1) and the thin solid line plotted in figure 13. Since the parameters found from the TAMTAM and ITD fits are very close, it is not surprising that both the fit (trap parameters from table 1, peak 1) and the simulation lines (trap parameters from table 3) are very close and reproduce remarkably well all the experimental points.

The ltTL glow curve of BaF_2:Ce in the vicinity of the V_k peak is shown by experimental points in figures 14(a) and 14(b) to which the same thermal lag of 1.7 K was applied. In figure 14(a) we show by a short dashed line a TAMTAM fit to experimental points that yields trap parameters shown in table 2, peak 1. The fit line matches experimental points very well, as expected, but the dashed first order line that was calculated from equations (3) assuming $K = 0$ and the s and E values of V_k-I, does not. Notably this line, which in figure 13 reproduces so well the experimental glow curve of BaF_2, falls entirely inside the curve defined by experimental points of BaF_2:Ce pointing again to the difference between the glow curves of the undoped and Ce-doped materials. The thick solid line represents the best attempt to reproduce the experimental glow curve by using equations (3) with the largest possible value of the parameter K, which we found to be 0.1. Unfortunately the improvement over the first order curve is not at all impressive and the overall match to experimental points remains rather poor. Model I fails to explain the shape of the TL glow curve in BaF_2:Ce.

In figure 14(b) we test therefore the model II. We assume, consequently, that there are two, not just one, traps in BaF_2:Ce. The first one is unique and occurs in both BaF_2 and BaF_2:Ce (V_k-I) while the second one, V_k-II, is characteristic only of BaF_2:Ce. In addition to the experimental points of BaF_2:Ce we show therefore two simulated first order glow curves ($K = 0$) that were calculated separately from equations (3) using parameters of two traps mentioned above. The areas under the calculated curves have been normalized to match that of the experimental BaF_2:Ce TL glow curve. In the next step we calculated the composite glow curve shown by a thick solid line, in which the contributions of the two component V_k curves were adjusted to achieve the best match to experimental points. We found a reasonably good match when the contribution of the V_k-II was set at 0.4 of that of V_k-I trap. Clearly model II provides better simulation of the BaF_2:Ce experimental TL glow curve than model I.

Since ITD curves are measured against time with constant temperature, to simulate ITD curves we rewrote equations (3) taking time t as an independent variable:

$$\frac{\partial n}{\partial t} = -\frac{n^2}{n+K} s \exp\left(-\frac{E}{k_B T}\right) \qquad I(\mathrm{T}) = \frac{n^2}{n+K} s \exp\left(-\frac{E}{k_B T}\right) \tag{6}$$

and used them to compare the predictions of the two models with experimental ITD results. In using the equations (6) at different temperatures T one should exercise caution since the value of the order parameter K depends on the initial concentration of filled traps n_0. This, in turn, may not, because of trap emptying, be equal to the value found from the TL fits or simulations. However, as long as the predetermined temperatures at which ITD curves have been measured are *below* the glow peak, the effect is small and can be safely neglected.

We begin with BaF_2. Since until now we have found neither an indication of the second trap nor higher order kinetics in BaF_2 we expect that the trap, V_k-I, that was used successfully to simulate the BaF_2 ltTL glow curve, will also provide a good simulation of the ITD curve. In figure 9(a) we compare therefore the experimental ITD curve (points) and a one-trap simulation shown by a thick solid line. This line represents the calculated ITD curve with no adjusted parameter (except for a multiplying factor and a background constant) using equations (6) with T set at 104 K and the trap parameters s and E equal to those of the V_k-I trap. Although

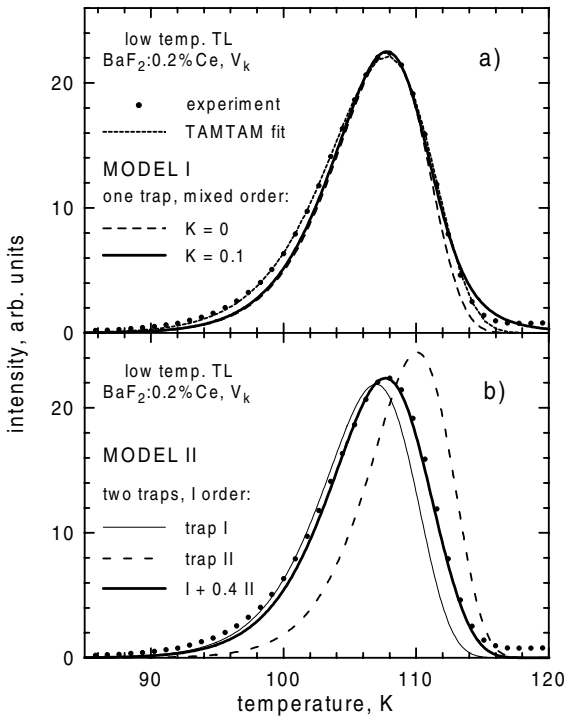

Figure 14. Thermoluminescence glow curves of BaF_2:0.2% Ce in the vicinity of the V_k peak following x-ray irradiation at 4 K. Heating rate was 9 K min^{-1}. Filled circles represent experimental points. In figure 14(a) a short dashed line depicts the TAMTAM fit to experimental points and long dashes and solid lines were calculated from model I assuming V_k-I trap parameters and only one adjustable parameter, K (see text). In figure 14(b) thin solid and dashed lines were calculated from model II assuming V_k-I and V_k-II trap parameters. The thick solid line is a composite of these two curves with distribution coefficients between the two traps as the only adjustable parameters (1:0.4).

the calculated curve has a slightly steeper slope than one would desire we note that only a marginal change of temperature by 0.3 K, to 103.7 K, is enough to obtain a very good agreement. Consistently we conclude again that the one-trap first order description of the thermally induced radiative recombination in BaF_2 is in a very good agreement with the experimental results.

We continue with BaF_2:Ce. In figures 9(b) and (c) we show the experimental and calculated ITD curves with no adjusted parameters except, as previously, for the scaling factor and the background. So, the dashed lines were calculated in the frame of model I (one trap, V_k-I) with the parameter K set at 0.1. We find that these lines clearly deviate from the experimental points. To obtain a good agreement the K parameter would have to be set to a value as high as 0.5 for the 103 K ITD curve and 0.4 for the 105 K curve. These high values would lead to unacceptably distorted TL glow curves. On the other hand the simulated curves shown by solid lines in figures 9(b) and (c), and calculated in the frame of model II (two traps, V_k-I and V_k-II) with fixed contributions (1 and 0.4) and trap parameters s and E from table 3, fall reasonably close to experimental points.

It is important to point out that the notion of the two different modes of V_k decay is not new. Beaumont *et al* [33] studied thermal annealing of V_k centres in CaF_2:Tm, SrF_2:Tm and

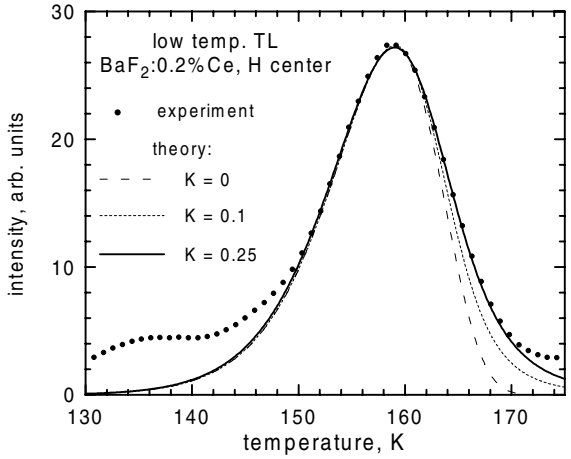

Figure 15. Thermoluminescence glow curve of BaF_2:0.2% Ce in the vicinity of the H peak following x-ray irradiation at 4 K. Heating rate was 9 K min^{-1}. Filled circles represent experimental points and lines represent various model calculations (see text).

BaF_2:Tm by monitoring the decay of the total EPR signal and, also by EPR methods, the thermally induced changes in the optically produced preferential alignment of the V_k centres. They note the occurrence of two different modes by which V_k centres decay; the first one preserves their orientation (0° linear motion) and the second does not (90° jump). In contrast to CaF_2:Tm and SrF_2:Tm, in BaF_2:Tm they found no measurable difference between activation energies of 0 and 90° jumps. They also found that the V_k reorientation in BaF_2:Tm follows formula (1) with $s = 3.2 \times 10^{12}$ s^{-1} and $E = 0.30 \pm 0.02$ eV. It is interesting to note that these estimates give values that fall between our estimates of parameters that characterize the two traps, V_k-I and V_k-II (table 3) the existence of which we have inferred from measurements of ltTL, ITD and synchrotron excited time profiles. We conclude therefore that these 'traps' represent simply two different modes of the V_k decay that are active in rare-earth-doped BaF_2.

In figure 15 we show the ltTL glow curve peak due to the H centres in BaF_2:Ce. This peak (compare figure 8) although almost totally absent in undoped BaF_2 becomes very prominent in the Ce-doped crystal as the concentration of compensating interstitial fluorine ions, capable of capturing a hole, increases strongly upon Ce doping. The first order simulation using equations (4) and trap parameters from the ITD fits (figure 12 and table 3), shown in figure 15 by a dashed line, reproduces reasonably well the position of the peak but not its shape. For higher values of the order parameter K the agreement improves and for $K = 0.25$ it is reasonably good.

The notion of the mixed order process in the case of the H centre receives further support from the ITD measurements. In figure 10 we show the ITD curve measured at 155 K. The simulated curves with no adjusted parameters (except of the scaling constant and the background) were calculated from equations (6) using the appropriate trap parameters from the ITD fits (figure 12 and table 3, trap H). At this particular temperature the trap lifetime is 58.5 s reasonably close to the value of 51.1 s that was derived from the two-exponential fit shown by a solid line. We note also that the first order simulation of the ITD curve with trap parameters from the (good) TAMTAM fit to the TL glow curve (yielding the 61.4 s lifetime at 155 K) fails to match the experimental points. While the first order line deviates from experimental points in both cases, the match between the mixed order simulation shown, for

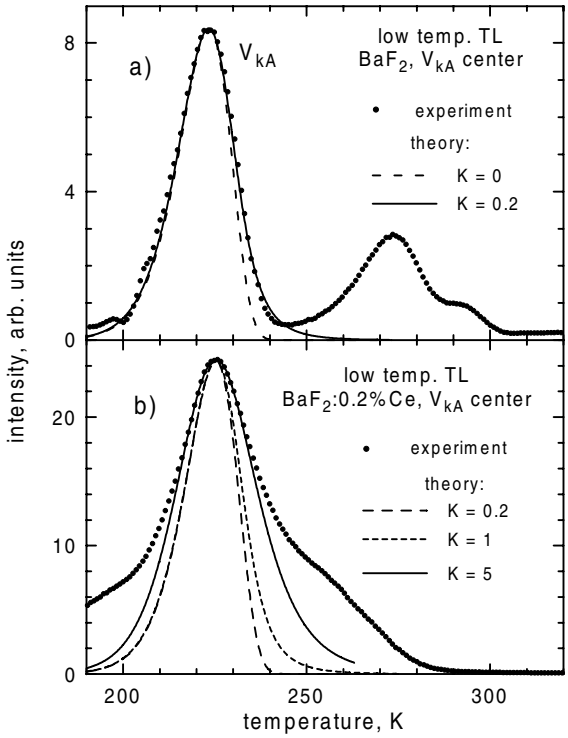

Figure 16. Thermoluminescence glow curve of (a) BaF_2 and (b) BaF_2:0.2% Ce in the vicinity of the V_{kA} peak following x-ray irradiation at 4 K. Heating rate was 9 K min^{-1}. Filled circles represent experimental points and lines represent various model calculations (see text).

$K = 0.25$, by a dotted line, and experimental points is much better. We conclude that, unlike the V_k centre, the H centres decay is not described very well by first order kinetics.

We note that these considerations can be used to set up an upper bound for the frequency factor of the H centre that we have previously assumed to be equal to that of the V_k-I trap. If the frequency factor was smaller than the one we have chosen, then, because the glow curve would be broader a smaller value of K would have to be taken to compensate for that. But then the agreement between the measured and calculated ITD curves would not be as good as it is now.

Finally in figure 16(a) and (b) we present ltTL glow curves in the range of the V_{kA} peaks in BaF_2 (figure 16(a)) and BaF_2:Ce (figure 16(b)). As in the previous case of the H centre the dashed line represents a first order simulation calculated from equations (3) with the V_{kA} trap parameters from the ITD fits (figure 12 and table 3). The better match is achieved in BaF_2 for $K = 0.2$. In BaF_2:Ce there is no good match even for K as high as 5 but in that case the much broader shape must come from the overlapping bands at both lower (at about 190 K) and higher (at about 250 K) temperatures. Since all of the three traps may decay and contribute to the ITD under, possibly, higher order kinetics the ITD curves are expected to be very complicated and have been omitted and not interpreted in the present paper.

3.4. Scintillation light yield (LY)

The results of scintillation light yield measurements on BaF_2:Ce are shown in figure 17. As explained in detail previously [24–28], each point represents a separate standard measurement

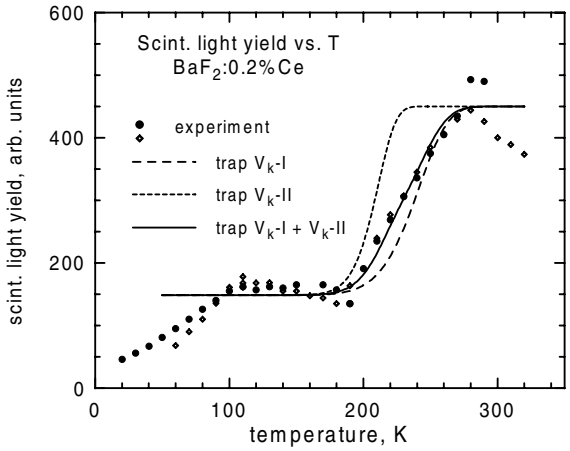

Figure 17. Scintillation light yield of BaF_2:0.2% Ce against temperature for a shaping time of 0.5 μs. Experimental points shown by filled circles and empty diamonds (two independent measurements on two different samples from the same boule) reflect the positions of photopeaks obtained under γ-excitation at various temperatures. The long and short dashed lines were calculated from a one-trap model (see text) with V_k-I and V_k-II trap parameters respectively, and the solid line was calculated from a two-trap model (model II, see text). With the exception of branching coefficients there are no other adjustable parameters (see text).

in which a scintillation pulse height spectrum is measured at a given temperature for a shaping time τ_{sh} of 0.5 μs. The position of the photopeak in such a spectrum, at least for the infinitely long integration time, corresponds exactly to the amount of scintillation light produced in an event in which all the energy of the incoming gamma particle has been deposited in the material and then transformed into light. Therefore it provides a very convenient measure of the scintillation light yield that can be used to characterize any given material. For an infinite integration time any thermally induced variations of the amount of light generated in the material would be exclusively due to thermally activated non-radiative processes such as those that govern the well known thermal quenching of luminescence. However, in practical measurements the integration time is never infinite (it is equal to $2.35\tau_{sh}$) and, on the other hand, the scintillation time profile usually contains trap-mediated contributions the decay times of which strongly depend on temperature. Therefore the measured curves depicting the scintillation light yield against temperature often show steplike features that are due to traps and each of which is well described by the following one-trap formula [24–26]:

$$\mathrm{LY}(T) = \mathrm{LY}_0 \left\{ a + b \frac{p(T)\tau_{rad}}{p(T)\tau_{rad} - 1} \left[1 + \frac{1}{p(T)\tau_{rad}} [\exp(-2.35\tau_{sh} p(T)) - 1] \right] \right\}. \tag{7}$$

In this formula LY_0 is the light yield of a 'trap-free' material, τ_{rad} is the Ce^{3+} radiative lifetime and $p = 1/\tau$ where τ is the trap lifetime (see formula (1)). The two terms in curly brackets represent normalized contributions from direct (a branching coefficient a) and trap-mediated (a branching coefficient b) recombination channels via Ce^{3+} ions. While the first represents the constant fraction of LY_0 (equal to a) the second is determined by the trap lifetime and the value of the shaping time τ_{sh} and is upper bound by a value of LY_0 b. Of course we also have $a + b = 1$.

The long and short dashed lines shown in figure 17 were calculated from formula (7) using parameters of the trap V_k-I and V_k-II, respectively, and for $a = 0.33$ and $b = 0.67$. The solid

line was calculated assuming that the total 0.67 trap contribution comes from the two traps not just one; the best fit was obtained for $b_1 = 0.5$ and $b_2 = 0.17$. We note that contributions of those two traps to the scintillation light yield, at 1 and 0.34, are not very different from those found from the ltTL glow curve analysis, at 1 and 0.4.

We conclude that the large increase of the scintillation light yield of BaF_2:Ce between 180 and 280 K is due to thermally induced detrapping of holes from the V_k centres. Interestingly the model calculations appear to support the notion of the two different complexes, V_k-I and V_k-II, that we have previously proposed in order to interpret results of ltTL and ITD measurements. Thermal decomposition of the V_k centres does follow two different routes that both contribute not only to the thermoluminescence at low temperatures but also to the scintillation light generated at ambient temperatures.

3.5. Scintillation and x-ray excited time profiles

In figure 18 we show by experimental points scintillation time profiles measured under gamma excitation as described before, at two different temperatures, 100 and 297 K. By solid lines we show the two calculated time profiles that used no adjustable parameters (except for the

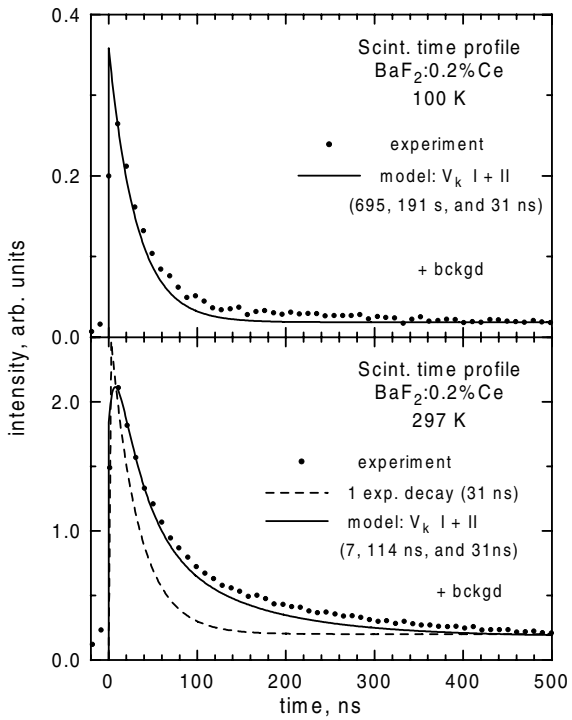

Figure 18. Scintillation time profiles of BaF_2:0.2% Ce at 100 and 297 K. Filled circles represent experimental points; solid lines were calculated from model II (two traps, V_k-I and V_k-II, see text). The trap lifetimes calculated at a given temperature are indicated in the figure. The dashed line represents a one-exponential decay with the Ce^{3+} radiative lifetime of 31 ns. With the exception of the fitting constant to correct for background there are no other adjustable parameters. Note that the model explains room temperature disparities between photoluminescence and scintillation time profiles of BaF_2:Ce at room temperature.

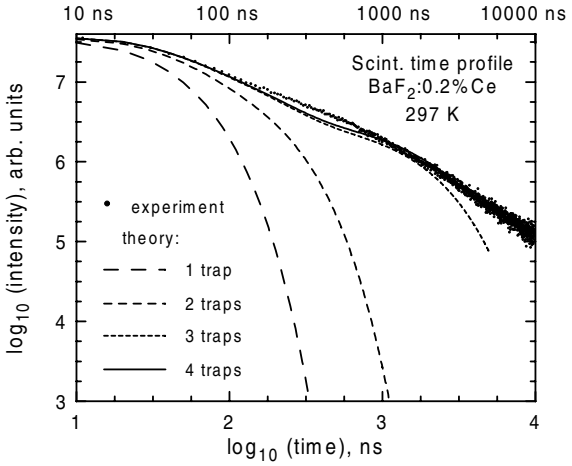

Figure 19. Scintillation time profile of BaF_2:0.2% Ce at 297 K on a 10 μs time scale. Small filled circles represent experimental points while lines represent calculated profiles that include varying number of traps. The only parameters varied were the branching coefficients (see text).

scaling factor and the background) according to the following formula [25]:

$$I(t) = a\,\exp\left(-\frac{t}{\tau_{rad}}\right) + b_1\frac{\tau_{rad}}{\tau_1 - \tau_{rad}}\left[\exp\left(-\frac{t}{\tau_1}\right) - \exp\left(-\frac{t}{\tau_{rad}}\right)\right] + b_2\frac{\tau_{rad}}{\tau_2 - \tau_{rad}}\left[\exp\left(-\frac{t}{\tau_2}\right) - \exp\left(-\frac{t}{\tau_{rad}}\right)\right] \tag{8}$$

where τ_1 and τ_2 are the lifetimes of the two traps, V_k-I and V_k-II, respectively, calculated using the appropriate trap parameters and at an appropriate temperature. The values of branching parameters are those found from the LY–T experiment ($a = 0.33$, $b_1 = 0.5$, $b_2 = 0.17$). Since at the lower temperature (100 K) the trap lifetimes at 695 and 191 s are very long they do not contribute either to the LY (that stands at the mere 0.33 of its maximum value) or to the scintillation time profile that shows a decay with the time constant of 31 ns (the direct component). For higher temperatures (297 K) the time profile changes strongly; the trap lifetimes reach now values as short as 7 and 114 ns and the profile displays a decay that is clearly slower than the one shown by a dashed line and decaying with the Ce^{3+} radiative lifetime of 31 ns.

Finally in figure 19 we show scintillation time profiles measured at the much longer time scale of 10 μs at 297 K. The solid lines show profiles calculated from formula (8) that was extended to include more traps; starting from 1 (the V_k-II trap only) then consecutively traps V_k-I, H′ and H are added. Since we have no information on participation of H′ and H traps in the scintillation we have chosen to vary parameters b_3 and b_4 describing their contributions to reach the best possible agreement with the experiment. The values of parameters a, b_1, b_2 are those found from the LY–T experiment (0.33, 0.5, 0.17) and b_3, b_4 are 1.6 and 2, respectively. These values are much higher than the appropriate contributions of respective traps to the ltTL spectra but this may be due to some inherent limitations imposed by our approach. First it is likely that under prolonged irradiation needed to reliably record thermoluminescence we may have saturated some of the peaks (e.g. those that are controlled by inadvertent impurities) and, therefore, obtain a distorted spectrum that has little to do with the one we would obtain under extremely short gamma irradiation that precedes scintillation. Also, as evident from figure 12,

our approach is reasonably accurate only in the case of the two traps, V_k-I and V_k-II. A good illustration is provided by comparison of decay times predicted by the model (figure 12 and table 3) and measured from the x-ray excited profiles. The points corresponding to decay times measured under modulated x-ray excitation as described before do not fall far off the straight lines assigned to V_{kA} centres and certainly confirm the validity of the model. On the other hand, although the agreement in the case of the shorter component is remarkably good, the difference between the measured and predicted decay times of the longer component (at 17 and 7 ms, respectively) is large enough to create problems in any detailed calculations of time profiles.

4. Conclusions

In the course of this work we have established a close link between radiation-induced centres, such as V_k, H′, H, V_{kA}, and $V_{kA'}$ and basic scintillation parameters such as the scintillation light yield and scintillation time profiles in BaF_2:Ce. This link clearly goes beyond the well established view that has been expressed so often in the past: '. . .in the case of scintillators, radiation effects are first observed in the optical transmission properties of the materials, and not in the scintillation process itself: an apparent decrease in the scintillation yield is likely due to increased self-absorption of the scintillation photons. . .' [47].

Interestingly we find that all these centres, V_k, H′, H, V_{kA} and $V_{kA'}$, some of which are the primary products of ionizing radiation that precede the formation of more stable radiation defects, also play an important and active role in the scintillation process itself determining both its speed and efficiency. Formally the role of these centres is equivalent to the role played by traps in systems in which the light is produced by radiative recombination of separated charge carriers. In reality the physical mechanism behind the 'trapping' phenomena is the impurity controlled or self-trapping of charge carriers in the host material, BaF_2:Ce in our case.

By adding new experiments that are specifically related to scintillation studies of detector materials (measurements of scintillation light yields and time profiles) and have not been used in research aimed at radiation defects themselves we have been able to obtain new information about those defects. In particular we have been able to confirm the existence of two different modes of the V_k decay and characterize them quantitatively by assigning to them numerical values of activation energies and preexponential factors.

The most important conclusions, however, are those that address the mechanisms of scintillation in BaF_2:Ce and, incidentally, in other rare-earth-doped alkaline earth fluorides. We have presented strong arguments that the dominant mechanism in BaF_2:0.2% Ce is the radiative recombination of separated charge carriers generated by ionizing radiation. The details of the process are presented below.

The dominant part of the scintillation light produced in BaF_2:0.2% Ce gathered and detected in the 0.5 μs time window, at about 67% of the total, is due to recombination of self-trapped mobile holes and Ce^{2+} ions that have previously captured electrons. Of all these holes about 75% is released by a mode that does not preserve their orientation (90° jump, V_k-I) and which completely dominates the thermally induced recombination (thermoluminescence) in undoped BaF_2. This mode is governed by first order kinetics and is, very likely, due to recombination of V_k centres and Ce^{2+} ions (V_k centres and F centres in BaF_2) that were originally located close to each other. Although the Catlow mechanism followed by recombination that failed to produce scintillation light (due to unfavourable configuration of closely spaced V_k and Ce complex) might be responsible for such a course of events we note that it also could be triggered by a self-trapped exciton collapse that decomposed in the neighbourhood of the Ce^{3+} ion.

The remaining 25% of all the holes that self-trapped in the initial stages of the scintillation process are released through the second mode of the V_k thermal decomposition (linear 0° jump, V_k-II) that we have identified in the Ce-doped BaF_2 and which is conspicuously absent in BaF_2. As these holes require a higher frequency factor (longitudinal vibrations are likely to have higher frequencies than transverse ones) and higher energies to move forward, they are, very likely, located further away from the Ce^{2+} ions and have to cover some distance before they are able to recombine. Clearly in the early stages of the scintillation process the initial locations of these holes and corresponding electrons are not space correlated. While the holes self-trap the electrons are captured by Ce^{3+} ions totally independently of holes, as proposed by Catlow [23]. The absence of such a process in undoped BaF_2 would suggest that, as noted previously, the electron 'self'-trapping process requires preliminary weak trapping of conduction band electrons that is missing in undoped, good quality BaF_2 [23].

Finally we have also demonstrated that there is a relatively large direct component, at about 33% of the total light, that originates, most likely, in the process in which the Ce^{3+} ions promptly capture valence band (!) holes despite the self-trapping although it is not likely that there is a related valence band hole charge transport over significant distances.

An improvement of the BaF_2:Ce scintillator would require that self-trapping of holes and trapping of electrons be eliminated or minimized in order to maximize the direct component decaying with the radiative lifetime of the Ce^{3+} ion. This, however, may prove difficult as both processes are intrinsic to the fluorite host doped with Ce. To minimize hole self-trapping we would have to increase the concentration of Ce ions. That would help to increase the fraction of holes that are captured by the Ce ions and do not self-trap. On the other hand, an increased Ce doping, besides contributing to some undesired energy migration and transfer processes, would also increase the fraction of electrons that are captured by the Ce ions. This would, unfortunately, lead to charge separation and, consequently, slower components or even a loss of the scintillation light.

Acknowledgments

This work was supported by the Polish Committee for Scientific Research (KBN) under the grant No 2P03B04914, by the European Community under the TMR contract ERBFMGECT950059, by the US Department of Energy (grant Nos DE-FG02-96-ER82117 and DE-FG-02-90-ER61033) and by ALEM Associates, Boston. We are also very grateful to Professor G Zimmerer and Dr M Kirm of HASYLAB, Hamburg, Germany, for their hospitality and help in VUV experiments at Superlumi station, and to Dr T M Piters of Universidad de Sonora, Hermosillo, Mexico, who developed and let us use the TL-fitting procedure TAMTAM.

References

[1] Weber M J, Bliss M, Craig R A and Sunberg D S 1995 *Radiation Eff. Defects Solids* **134** 23
[2] Cherry S R 1994 *Nucl. Instrum. Methods* A **348** 577
[3] Moses W W and Derenzo S E 1996 *Proc. Int. Conf. on Inorganic Scintillators and Their Applications, SCINT95* ed P Dorenbos and C W E van Eijk (Delft: Delft University Press) pp 9–16
[4] Lecoq P 1996 *Proc. Int. Conf. on Inorganic Scintillators and Their Applications, SCINT95* ed P Dorenbos and C W E van Eijk (Delft: Delft University Press) pp 52–61
[5] Novotny R 1996 *Proc. Int. Conf. on Inorganic Scintillators and Their Applications, SCINT95* ed P Dorenbos and C W E van Eijk (Delft: Delft University Press) pp 70–2
[6] Dorenbos P, de Haas J T M, Visser R, van Eijk C W E and Hollander R W 1993 *IEEE Trans. Nucl. Sci.* **40** 424
[7] Halliburton L E and Edwards G J 1994 *Mater. Res. Soc. Symp. Proc.* vol 348, ed M J Weber, P Lecoq, R C Ruchti, C Woody, W M Yen and R Zhu (Pittsburgh, PA: Materials Research Society) pp 423–34

[8] Kimura K and Hong W 1998 *Phys. Rev.* B **58** 6081
[9] Vail J M, Emberly E, Lu T, Gu M and Pandey R 1998 *Phys. Rev.* B **57** 764
[10] Czirr J B and Catalano E 1977 *Nucl. Instrum. Methods* **143** 487
[11] Farukhi M R and Swinehart C F 1971 *IEEE Trans. Nucl. Sci.* **18** 200
[12] Taylor R C, Nestor O H and Utts B 1986 *IEEE Trans. Nucl. Sci.* **33** 243
[13] Dorenbos P, Visser R, van Eijk C W E, Hollander R W and den Hartog H W 1991 *Nucl. Instrum. Methods* A **310** 236
Visser R, Dorenbos P, van Eijk C W E, Hollander R W and Schotanus P 1991 *IEEE Trans. Nucl. Sci.* **38** 178
[14] Andriessen J, Dorenbos P and van Eijk C W E 1991 *Mol. Phys.* **74** 535
[15] Visser R, Dorenbos P, van Eijk C W E, Meijerink A, Blasse G and den Hartog H W 1993 *J. Phys.: Condens. Matter* **5** 1659
[16] Visser R, Andriessen J, Dorenbos P and van Eijk C W E 1993 *J. Phys.: Condens. Matter* **5** 5887
[17] Hayes W 1974 *Crystals with the Fluorite Structure* (Oxford: Clarendon)
[18] Song K S and Williams R T 1993 *Self-Trapped Excitons* (Berlin: Springer)
[19] Merz J L and Pershan P S 1967 *Phys. Rev.* **162** 217
[20] Williams R T, Thoma E D and Bunton P H 1994 *Mater. Res. Soc. Symp. Proc.* vol 348 ed M J Weber, P Lecoq, R C Ruchti, C Woody, W M Yen and R Zhu (Pittsburgh, PA: Materials Research Society) pp 331–42
[21] Wojtowicz A J, Glodo J, Wisniewski D and Lempicki A 1997 *J. Lumin.* **72–74** 731
[22] Thoma E D, Yochum H M and Williams R T 1997 *Phys. Rev.* B **56** 8001
[23] Catlow C R A 1979 *J. Phys. C: Solid State Phys.* **12** 969
[24] Wojtowicz A J, Drozdowski W, Wisniewski D, Wisniewski K, Przegietka K R, Oczkowski H L and Piters T M 1998 *Radiat. Meas.* **29** 323
[25] Wojtowicz A J, Glodo J, Drozdowski W and Przegietka K R 1998 *J. Lumin.* **79** 275
[26] Wojtowicz A J, Glodo J, Lempicki A and Brecher C 1998 *J. Phys.: Condens. Matter* **10** 8401
[27] Lempicki A and Bartram R H 1999 *J. Lumin.* **81** 13
[28] Wojtowicz A J 1999 *Acta Phys. Pol.* A **95** 165
[29] Glodo J, Szupryczynski P and Wojtowicz A J 1999 *Acta Phys. Pol.* A **95** 259
[30] Zimmerer G 1991 *Nucl. Instrum. Methods Phys. Res.* A **308** 178
[31] `http://www-hasylab.desy.de/facility/experimental_stations/stations/`; see the I-beamline
[32] Rodnyi P A 1997 *Physical Processes in Inorganic Scintillators* (New York: Chemical Rubber Company)
[33] Beaumont J H, Hayes W, Kirk D L and Summers G P 1970 *Proc. R. Soc.* A **315** 69
[34] Williams R T, Kabler M N, Hayes W and Stott J P 1976 *Phys. Rev.* B **14** 725
[35] Shi C, Kloiber T and Zimmerer G 1988 *J. Lumin.* **40/41** 189
[36] Rubloff G W 1972 *Phys. Rev.* B **5** 662
[37] Loh E 1967 *Phys. Rev.* **154** 270
[38] Shi C, Kloiber T and Zimmerer G 1990 *Phys. Scr.* **41** 1022
[39] Wojtowicz A J, Drozdowski W, Glodo J and Wisniewski D 1999 *Hasylab Annual Report '98* `http://www-hasylab.desy.de/science/annual_reports/1998/index.html`
[40] Atobe K 1979 *J. Chem. Phys.* **71** 2588
[41] Ershov N N, Zakharov N G, Reiterov V M and Rodnyi P A 1982 *Opt. Spectrosc.* **52** 222
[42] Zakharov G N, Kkhudro A Kh, Mel'chakov E N, Rodnyi P A and Yanovskii V V 1992 *Sov. Phys.–Solid State* **34** 803
[43] Hayes W and Lambourn R F 1973 *J. Phys. C: Solid State Phys.* **6** 11
[44] Call P J, Hayes W, Stott J P and Hughes A E 1974 *J. Phys. C: Solid State Phys.* **7** 2417
[45] Randall J T and Wilkins M H F 1945 *Proc. R. Soc.* A **184** 366
[46] McKeever S W S 1985 *Thermoluminescence of Solids* (Cambridge: Cambridge University Press) pp 45–48, 66
[47] Caffrey A J, Heath R L, Ritter P D, Van Siclen C DeW, Anderson D F and Majewski S 1986 *IEEE Trans. Nucl. Sci.* **33** 230